EFFECT OF ADDITION OF ZrO_2, TiO_2, and $ZrTiO_4$ OXIDES ON MICROSTRUCTURE AND MECHANICAL PROPERTIES OF CAST 7075 ALUMINUM

Devang Mahant Research Scholar, Department of Metallurgical & Materials Engineering, Faculty of Technology and Engineering, The M. S. University of Baroda Vadodara, 390001, India and Government Engineering College, Gandhinagar, 382028, India.
Dr. Vandana Rao Associate Professor, Department of Metallurgical & Materials Engineering, Faculty of Technology and Engineering, The M. S. University of Baroda Vadodara, 390001, India.

Abstract
Wrought 7075 aluminum alloy has the highest mechanical properties as compared to other aluminum alloys. But, cast 7075 aluminum alloy shows an entirely different result due to solute segregation phenomena at the grain boundaries. To avoid solute segregation, many strategies are employed, such as mold vibration, the use of heat treatment cycles, and the addition of chemicals to control the solidification rate. Out of all the techniques, chemical treatment with the oxide addition generates more nuclei for better distribution of segregated phase is quite easier than the rest. It is quite similar to adding inoculants to the liquid melt to alter the microstructure. To improve the mechanical properties of cast 7075 aluminum alloy, 2.5 wt.% of oxides like ZrO_2, TiO_2, and $ZrTiO_4$ were added. The powder particles are in the range of ~ 2 to 6 μm in size. The prepared liquid melt was poured into a metal die. The 2.5 wt.% ZrO_2 added Al 7075 shows good mechanical properties in comparison to as-cast Al 7075. The hardness of 2.5 wt.% ZrO_2 added Al 7075 shows double the value compare to as-cast Al 7075. It also shows uniform distribution of the segregated phase mentioned in the micrograph. The XRD analysis confirms the presence of intermediate phases $\eta(Mg(AlCuZn)_2)$.

Keywords: 7075 aluminum alloy, oxide addition, Microstructure, Mechanical properties, SEM-EDS

Introduction
T6 heat-treated 7075 alloys have wide potential in the field of automobiles due to their best mechanical properties. To reduce fuel consumption and increase vehicle performance, a lightweight-to-high strength ratio is very important worldwide (Imran & Khan, 2019). To improve the cast properties of 7075 alloys, several techniques are investigated. It is categorized into three major sectors; the addition of oxides, modification of the heat treatment cycle, and the microalloying effect (ALTUNTAŞ, 2022; Sabbar et al., 2021). The major one includes the addition of nanoparticles made of oxides, carbides, and nitrides. The addition of Al_2O_3, TiO_2, TiC, SiC, AlN, etc are investigated by several researchers (Gan et al., 2014; Karunanithi et al., 2014; Yang et al., 2019; Zhai et al., 2020; P. X. Zhang et al., 2019; Zuo et al., 2019). The second technique includes a heat treatment cycle named the diffusion-controlled solidification process (Parsania et al., 2015; Rao et al., 2012). The microalloying effect includes grain refinement of cast alloy by the addition of a small quantity of Zr, Sc, Sr, Ag, Er, Ti-B_2, and other rare earth metals (A. Ghosh et al., 2020; He et al., 2010; T. Li et al., 2015; Vlach et al., 2020; Wang et al., 2011; W. L. Zhang et al., 2019). The 7XXX series aluminum alloy has Zn, Mg, Cu, and Cr solutes. The solute distribution during solidification leads to micro-segregation and the formation of coarse intermetallic particles, which can significantly influence the properties of the 7000 series aluminum alloys. The strength of these alloys generally depends on Zn to Mg ratio. It has the problem of hot cracking during rapid cooling along with the presence of Zn concentration of around 7 to 8 wt.% (Senkov et al., 2005). The as-cast microstructure involves α(Al), eutectic of $(\alpha(Al)+Mg(Al,Cu,Zn)_2$, and Al_7Cu_2Fe phases (X. G. Fan et al., 2006). The small addition of Zirconium can improve its properties by forming metastable and coherent Al_3Zr dispersoids, which prevent recrystallization through a grain boundary pinning mechanism (Morere et al., 2001). Furthermore studied the microstructure-property relationship of TiO_2 reinforced AA7075 MMC via stir cast and found the density and porosity increased with the increasing amount of TiO_2 (Alagarsamy & Ravichandran, 2019).
Solidification of 7XXX series aluminum alloy shows the presence of some intermetallic particles such as Al_6CuMg_4, $Al_2Mg_3Zn_3$, AlCuMg, $MgZn_2$, and Al_2Cu (X. Fan et al., 2006; X. G. Fan et al., 2006; Mondal & Mukhopadhyay, 2005). These intermetallic phases have low melting points and

create problems while hot working (Reza et al., 2011). The main hardening elements Zn, Mg, and Cu play an important part in the formation of the intermediate phases such as η($MgZn_2$), S(Al_2CuMg), and T(AlCuMgZn), which control the final properties (Starink & Li, 2003). Some other minor additive elements like Ti, Zr, Fe, and Si will also influence the microstructure by forming different intermetallic phases at different locations (Osamura et al., 1996; Park & Ardell, 1988; Yazdian et al., 2010). While solidification dendrites are observed and at the end of the dendrites segregation of alloying elements is also observed which controls the final mechanical properties of cast alloys (Anyalebechi, 2004). The main focus of the present study is to alter the microsegregation pattern to enhance the mechanical properties by the addition of 2.5 wt.% ZrO_2, TiO_2, and $ZrTiO_4$ into the cast Al 7075 alloy. The addition of oxide of Zr & Ti influences the dendrites of alpha aluminum and changes the distribution pattern of intermetallic phases which finally improves the mechanical properties of cast Al 7075 alloy. The combined effects of Zr & Ti oxide are ineffective to modify the microstructure.

Experimental Procedure

In a resistance heating furnace as shown in Fig. 1(a) with a 2 kg capacity of graphite crucible, the 7075-T6 aluminum alloy was melted. After degassing and impurity removal, 2.5 wt.% ZrO_2, TiO_2, and $ZrTiO_4$ were added. The size of the powder particle was measured by SEM analysis using a scale bar in Fig. 2(a) to Fig. 2(f), the average particle size varies between 2 to 6 µm. The melting was carried out at 720 °C. Manual stirring was done for 2 to 3 minutes to avoid the float of the oxide particles and increase interaction between oxide particles and liquid melt by using a pure aluminum rod. The liquid metal was poured into the metallic mold of cast iron after the addition of the oxide. Fig. 1(b) and Fig.1(c) indicate the dimensions of the die and actual sample after solidification respectively. The final size of cast rods is Ø 20 mm and 170 mm long. Sampling was done for characterization like chemical analysis, microscopy, tensile strength, hardness, etc. Fig. 1(d) and 1(e) indicate the prepared sample for the above characterization. Chemical analysis was carried out by mass Spectroscopy and Energy Dispersive Spectroscopy (EDS) method. Standard metallography procedures were followed to prepare the microstructure and etched with diluted 0.5 percent HF solution. The presence of Zr, Ti, and Zr& Ti both together" in the samples was determined using EDS analysis. For SEM-EDS and microscopic analysis the JOEL JSM-5610LV and Olympus GX41 machines were used. The grain size was measured using an image analyzer as per ASTM E112. Brinnel hardness and micro-hardness tester were used to determine the hardness value of the samples based on an average of six readings. Tensile testing was carried out on the Monsanto-20 tensile testing machine has a crosshead speed of 0.5 mm/min. The ultimate tensile strength, % elongation, and % RA were measured based on an average of three readings. The dimensions of the tensile testing specimen prepared according to ASTM E8M with a gauge length five times the diameter is shown in Fig. 1(d).

Resistance Heating Furnace Set up

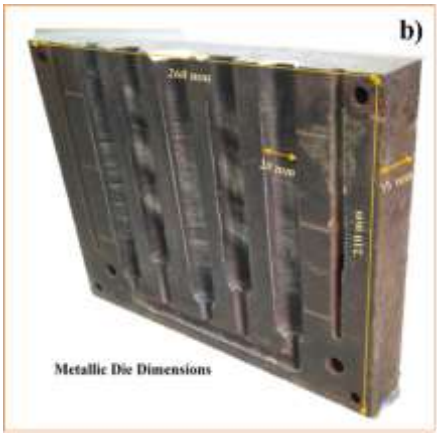

Metallic Die Dimensions

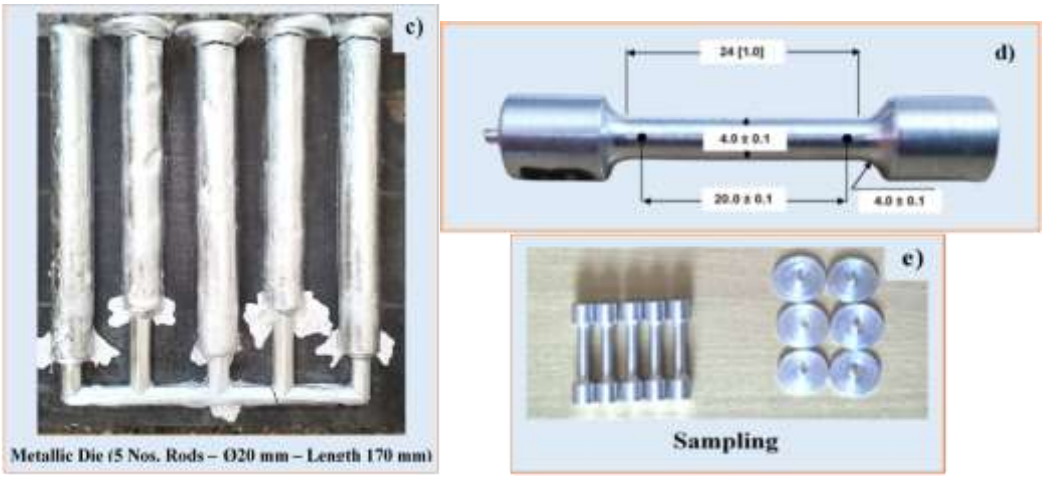

Fig. 1 Experimental set-up and sampling plan a) resistance heating furnace; b) metallic die dimensions; c) cast sample dimension; d)tensile specimen dimensions as per ASTM E8M;e) sampling.

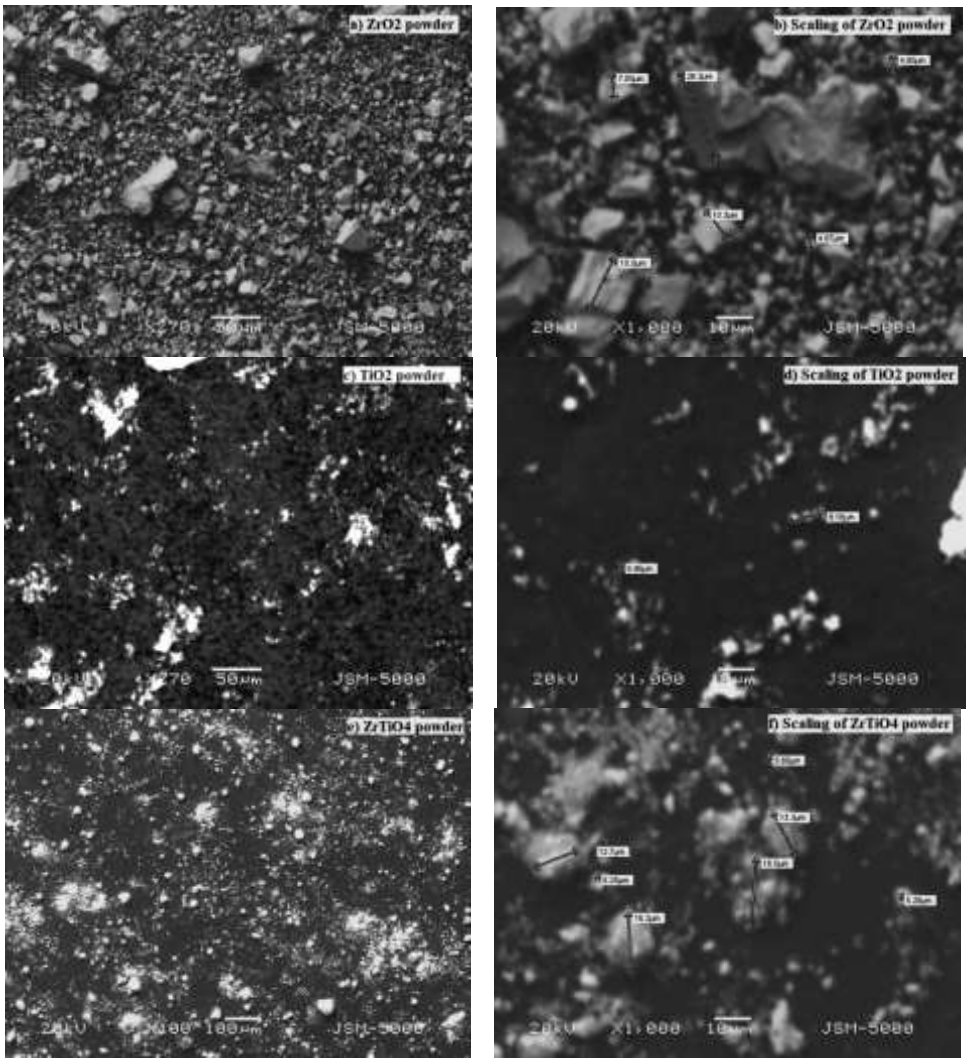

Fig. 2 SEM (scanning electron microscope) image and particle size measurement of oxide powder a) ZrO_2 Powder; b) scaling of ZrO_2 powder; c) TiO_2 powder; d) scaling of TiO_2 powder; e) $ZrTiO_4$ powder; f) scaling of $ZrTiO_4$

Results and Discussion

Chemical analysis of the as-received 7075 aluminum alloy

The mass spectroscopy technique was used to examine the chemical analysis of the 7075-T6 aluminum alloy. Three distinct samples from a single batch were analyzed, and the average findings are shown in Table1. Chemical compositions are in the range of 7075 aluminum alloy.

Table 1 Chemical analysis of the as-received 7075-T6 aluminum alloy.

Element (wt. %)	Zn	Mg	Cu	Mn	Al
Average	5.48	2.25	1.54	0.09	90.64

Chemical analysis of oxides powders

The chemical analysis of the as-received oxide powders is represented in Table 2. The ZrO_2 and $ZrTiO_4$ powders are pure, TiO_2 powder contains roughly 3.5 and 9.0 wt.% impurities of Ca and Si, respectively.

Table 2 Chemical analysis of received oxides powder by EDS analysis.

Oxide Powder (wt. %)	Zr	Ti	O
ZrO_2	64.61	---	35.39
TiO_2*	---	29.8	57.36
$ZrTiO_4$	25.20	25.10	49.71

*impurities such as Ca & Si in 3.42 & 9.24 wt. % respectively.

Chemical analysis of oxide added cast Al 7075

The mass spectroscopy examination of oxides added cast sample is presented in Table 3. It is carried out by Thermo Fisher Scientific model ARL™ iSpark 8860 Fire Assay machine.

Table 3 Spectroscopy analysis of Al 7075; a) as-cast, b) 2.5 wt.% added ZrO_2, c) 2.5 wt.% added TiO_2, d) 2.5 wt.% added $ZrTiO_4$.

System	Zn	Mg	Cu	Cr	Zr	Ti
			Element (wt.%)			
a	5.7223	2.4270	1.8060	0.2050	0.0101	0.0300
b	5.9810	2.2360	1.6180	0.2120	0.0118	0.0240
c	5.8821	2.2290	1.5490	0.2040	0.0103	0.0280
d	6.0630	2.2870	1.6780	0.2050	0.0115	0.0290

Mass spectroscopy confirmed the presence of Zr and Ti at the macroscopic level. Further, at the microscopic level presence of Zr and Ti was confirmed by EDS analysis and mentioned in Table 4.

Table 4 EDS analysis of Al 7075 with different condition like ; a) as-cast, b) 2.5 wt.% added ZrO_2, c) 2.5 wt.% added TiO_2, d) 2.5 wt.% added $ZrTiO_4$

Alloy System	Wt.% Zr	Wt.% Ti
A	---	---
B	0.04 – 0.22	---
C	---	0.01 – 0.05
D	0.36 – 0.77	0.03 – 0.04

Microstructure evolution of 7075 aluminum alloy after addition of oxides

The optical and SEM (BSE mode) micrographs are examined. The microstructure of as-cast 7075 aluminum alloy is shown in Fig. 3(a). It represents the major α(Al) phase which ends in the form of black boundaries made up of intermetallic phases. The intermetallic phases, η($MgZn_2$), T($Al_2Mg_3Zn_3$), S(Al_2CuMg), and θ(Al_2Cu) are the most typically found in the as-cast microstructure of the 7XXX series aluminum alloys (Ii et al., 2005; X. M. Li & Starink, 2001). Some of the intermetallic phases are also present at the center of the grains. At some portion of the micrograph, original columnar grains of the original cast structure is also present. The white portion denotes the α(Al) phase, while the black portions denote the intermetallic phase (Xie et al., 2003). The average

grain size of as-cast Al 7075 is 11 as per ASTM E112. The tensile property of as-cast 7075 Al alloy is reduced by a continuous network of thick eutectic phases in the form of intermetallic such as η($MgZn_2$), T($Al_2Mg_3Zn_3$), and S(Al_2CuMg), etc (Mondal & Mukhopadhyay, 2005). The presence of dispersoid particles leads to a change in the recrystallization behavior of alloy (G. Ghosh & Asta, 2005; Mondal et al., 2007; Pourkia et al., 2010; Sha & Cerezo, 2005). Oxide-added samples change the distribution patterns of the eutectic phase, as illustrated in Fig. 3(b), 3(c), and 3(d).

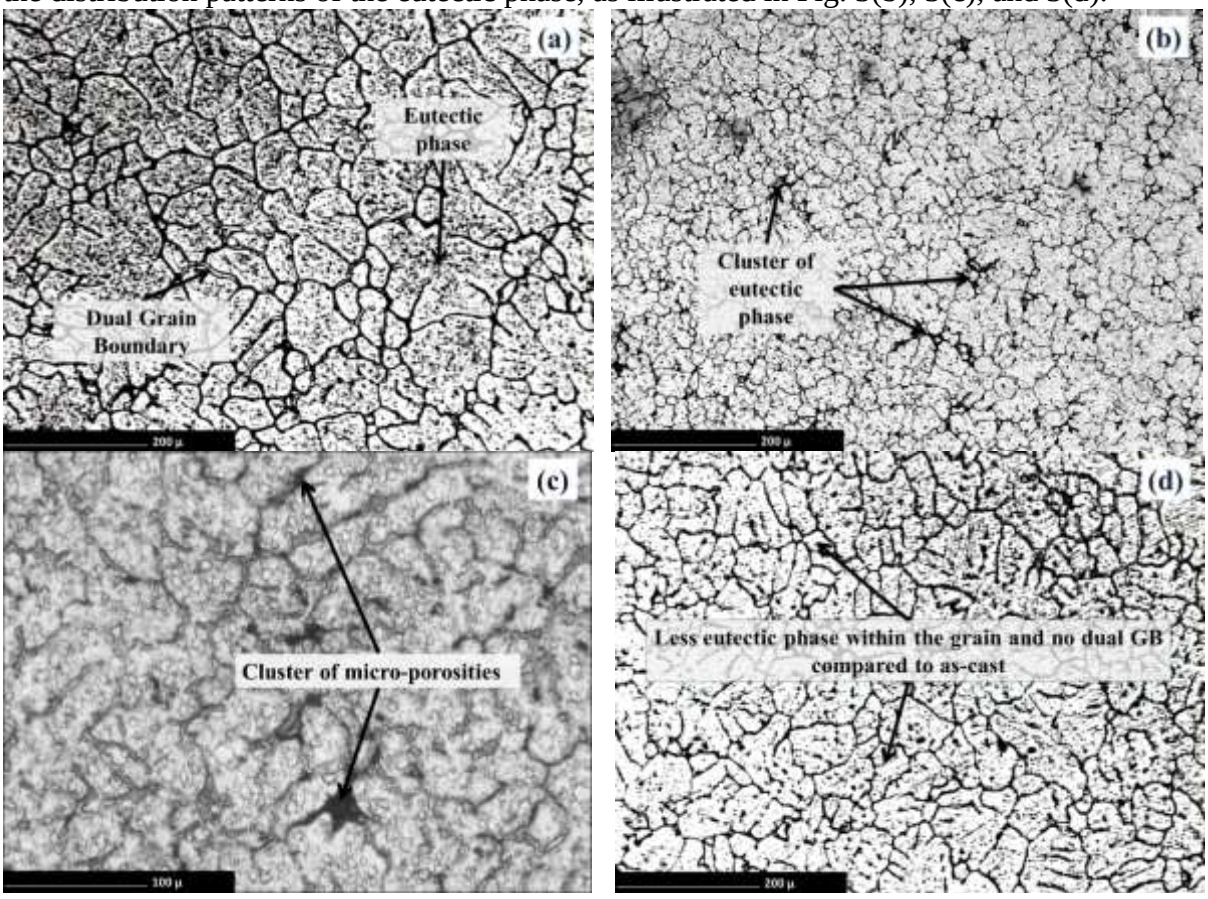

Fig. 3 the optical micrographs of 7075 aluminum alloy; a) as-cast, b) 2.5 wt.% added ZrO_2, c) 2.5 wt.% added TiO_2, d) 2.5 wt.% added $ZrTiO_4$.

The 2.5 wt.% ZrO_2 added sample indicates the presence of α(Al) and eutectic phase in the form of intermetallic. The microstructure shows a uniform grain boundary, a cluster eutectic phase at several regions, as well as a reduction in the size of α(Al) grains. The addition of Zr developed the Al_3Zr phase, which was coherent with the aluminum matrix, and is largely responsible for hindering the movement of dislocation and increasing the local dislocation density. As per several researchers' report, in the case of a multi-component system like 7075 alloy, the presence of the second phase are very complex and finally, it can control the mechanical and corrosion properties of the alloys (Mondal & Mukhopadhyay, 2005; Seyed Ebrahimi et al., 2010). The 2.5 wt.% ZrO_2 added sample changes the eutectic phase distribution pattern and improves tensile strength with a value of 196 MPa and hardness values of 112 BHN with the grain size of 12 as per ASTM E112. After the addition of 2.5 wt.% of TiO_2, hardness remains the same but the presence of clustered micro-porosities reduces the tensile properties as presented in fig. 3(c). The presence of impurities like calcium and silicon in TiO_2 powder may be the cause of micro-porosities. Chen et. al. reported significant improvements in strength and ductility at 1 wt.% Ti addition, but beyond 1 wt.% Ti addition is also decreased. It may be due to stress concentration, which easily takes place at the tips of thick aciculate or rod-like $TiAl_3$ phases. The presence of these stresses will lead to the de-bonding of the particle interface to micro-crack nucleation, propagation, and finally into brittle rupture (Chen et al., 2015). The micrograph of the TiO_2-added sample does not reflect the presence of any needle. Finally, the presence of impurities in TiO_2 powder like Si and Ca makes the brittle phase responsible for the brittle behavior of the sample. The 2.5 wt.% $ZrTiO_4$ added Al 7075 microstructure is shown in Figure 3(e) where coarse columnar grains with a slender solid solution within α(Al) grains and interdendritic intermetallic. The significant effect of the combined Zr & Ti oxide addition on cast Al 7075 was

nullified except for eutectic distribution. The measured grain size was 10 due to coarse columnar grains. Fractography analysis of tensile specimens of as-cast and oxide-added Al 7075 is shown in Fig. 5(a) to 5(d). The pattern of dimples and cleavage both are observed in Fig. 5(a) of as-cast Al 7075. The size reduction of the dendrite is very rarely observed and is not reported. The dimples show that ductility is remarkably high even in the cast. The backscattered mode Fig. 6(a) proves the less refinement of dendrites. The majority of the cleavage mode and some cracks can be seen in the fractography of ZrO_2 and TiO_2 added Al 7075 alloy as presented in Fig. 5(b) and 5(c) respectively, which significantly lowers the ductility value from 10% to 3%. The oxide added nuclei's reveals a reduction in the scale of the dendrites, as presented in Fig. 6(b) and 6(c). Fractography of $ZrTiO_4$ is shown in Fig. 5(d), where the presence of a dimple increases the ductility value just similar to as-cast sample. Backscattered Fig. 6(d) showed a very modest effect on nuclei generation, and as a result, very little dendritic refinement is observed.

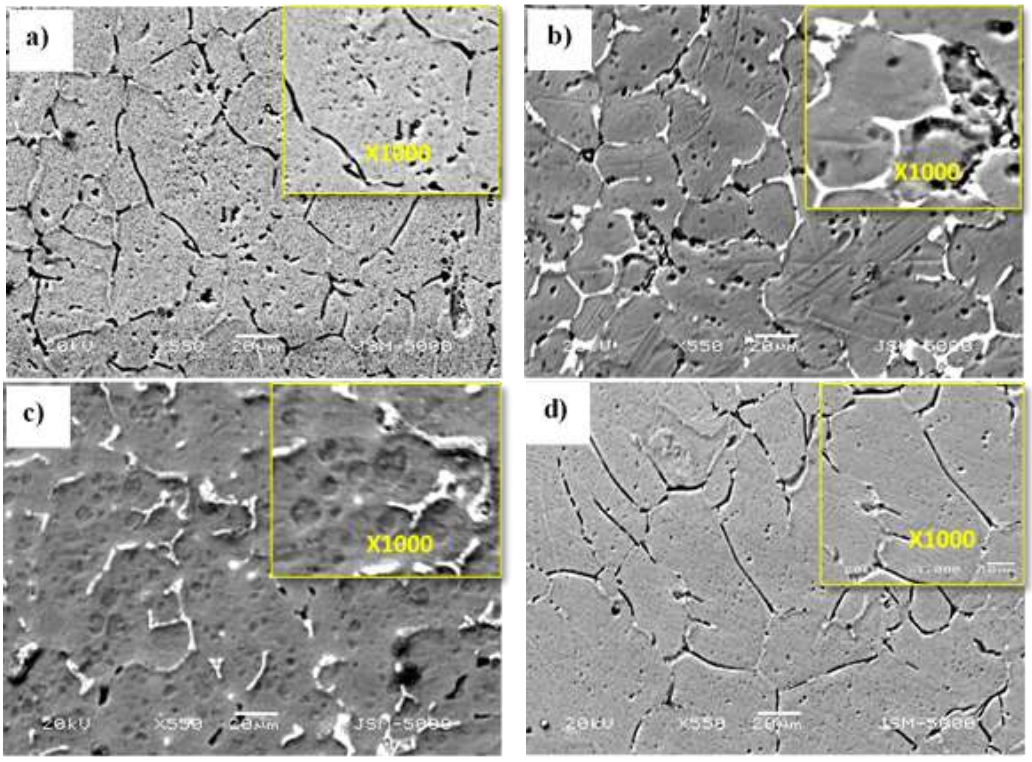

Fig. 4 the SEM micrographs of 7075 aluminum alloy; a) as-cast, b) 2.5 wt.% added ZrO_2, c) 2.5 wt.% added TiO_2, d) 2.5 wt.% added $ZrTiO_4$.

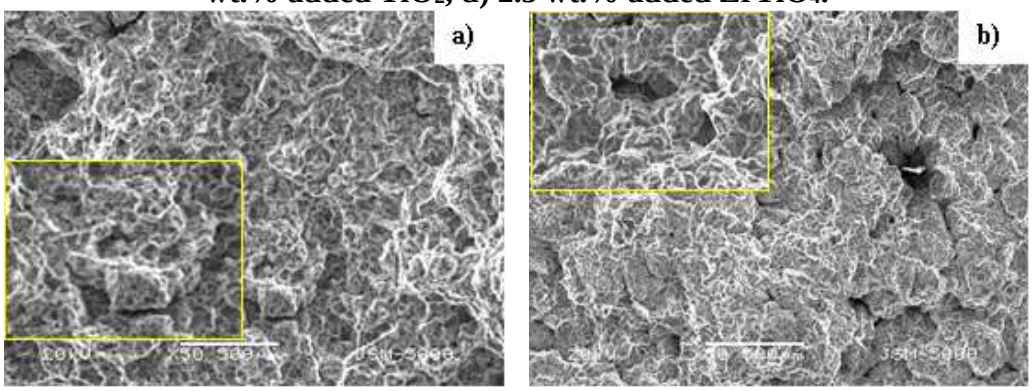

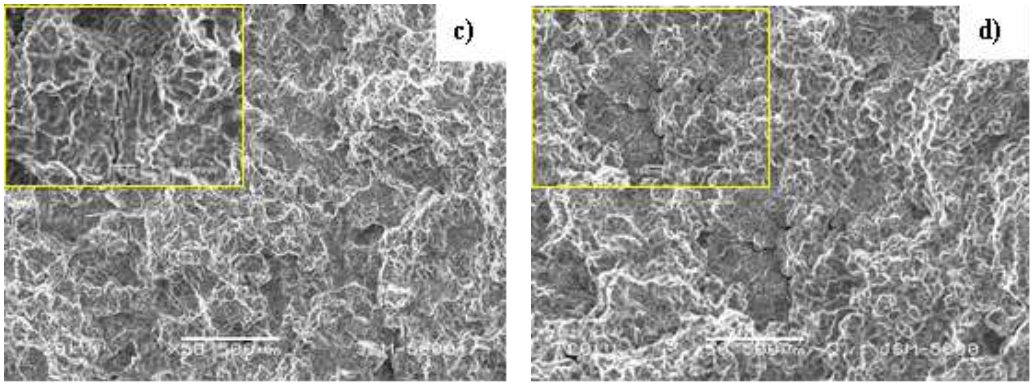

Fig. 5 Fractography analysis (SEM) of Al 7075; a) as-cast, b) 2.5 wt.% added ZrO_2, c) 2.5 wt.% added TiO_2, d) 2.5 wt.% added $ZrTiO_4$.

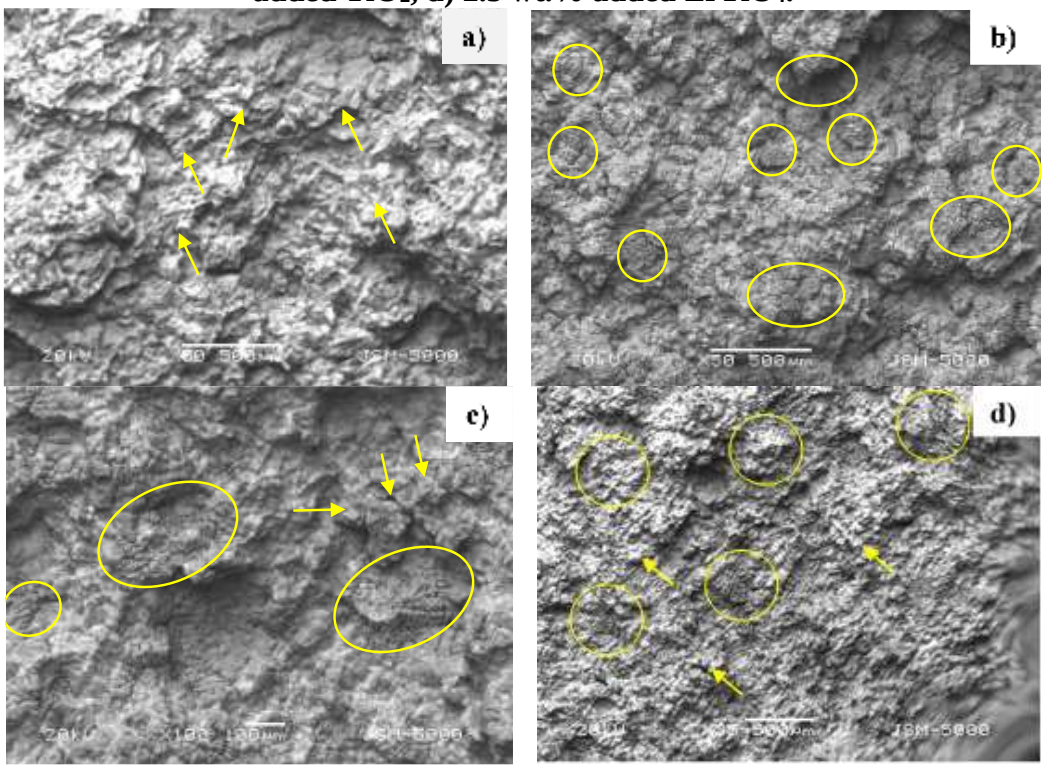

Fig. 6 Fractography analysis (SEM-BSE mode) of Al 7075; a) as-cast, b) 2.5 wt.% added ZrO_2, c) 2.5 wt.% added TiO_2, d) 2.5 wt.% added $ZrTiO_4$.

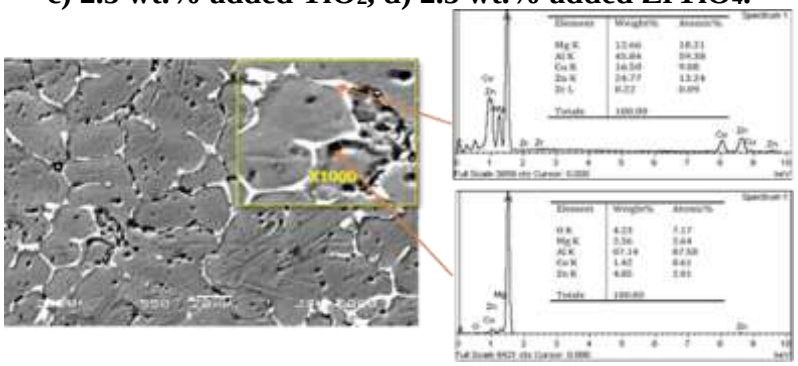

Fig. 7 SEM-EDS analysis of 2.5 wt.% ZrO_2 added 7075 aluminum alloy.

Fig. 4(a) shows the SEM micrograph of as-cast 7075 Al alloy. The primary solid solution is represented by grey, whereas the non-equilibrium eutectic solid solution is represented by dark. Within the α(Al) grains the presence of the non-equilibrium eutectic solid solution was also confirmed as black dots. Fig. 4(b) & Fig. 7 reveal finer α(Al) grains and bright areas that confirm the presence of 0.22 wt.% Zr in ZrO_2 added sample. While the presence of non-equilibrium eutectic solid solution was observed in dark areas, can be formed in the intermetallic phase such as η($MgZn_2$), T($Al_2Mg_3Zn_3$), S(Al_2CuMg), and θ(Al_2Cu). The SEM micrograph in Fig. 4(c) reveals the presence of porosity in various areas results in a decrease in tensile strength but no effect on hardness value. Fig. 4(a) and 4(d) show comparable SEM micrographs, the only variations are non-

equilibrium eutectic solid solution distribution and grain size, which result in a nearby value of tensile strength, elongation, and hardness. The non-equilibrium eutectic solid solution in α(Al) grains and between the interdendritic region is present in the as-cast 7075 Al alloy but in the case of 2.5 wt.% $ZrTiO_4$ added Al 7075 alloy and its amount decreased. The epitaxial lattice parameter of $Al_3(Zr, Ti)$ with the $L1_2$ structure compounds with α(Al) grains results in equiaxial and columnar grain growth due to the lack of nucleation events at the front of the growing solid-liquid interface (Tan et al., 2021; X. Zhang et al., 2022). Fig. 8 represents the XRD pattern of oxide added 7075 Al alloy. The basic XRD results are similar in all the cases but small peaks appeared due to the presence of oxide additions. It confirms the various intermetallics and non-equilibrium phases present as discussed earlier. Major phase confirms like η($Mg(AlCuZn)_2$) which also exist in a variety of the forms like η($MgZn_2$), T($Al_2Mg_3Zn_3$), and S(Al_2CuMg) (Kamali et al., 2022).

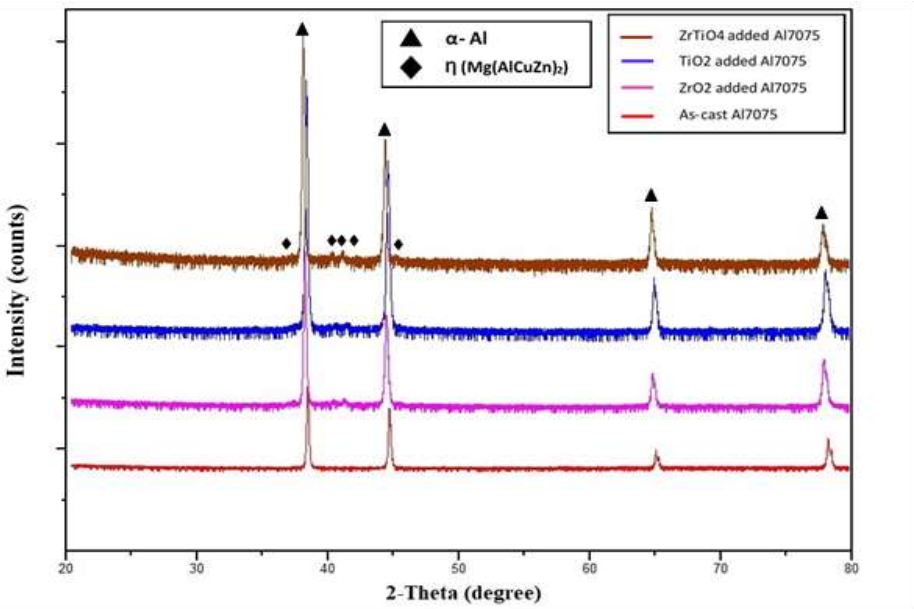

Fig. 8 XRD analysis of Al 7075; a) as-cast, b) 2.5 wt.% added ZrO_2, c) 2.5 wt.% added TiO_2, d) 2.5 wt.% added $ZrTiO_4$.

Mechanical properties

These samples are subjected to mechanical tests such as Brinell and microhardness along with tensile strength. The results of the test are given in Table 6. ZrO_2 added samples show a hardness of 112 BHN and which is 52% higher than the as-cast 7075 Al alloy. Microhardness value also becomes 56% higher than as-cast 7075 Al alloy. The uniform distribution of the non-equilibrium eutectic phase and the development of finer α(Al) grains due to the inhibition of recrystallization given by Al_3Zr dispersoids are the basis for the increase in hardness. The microhardness indentation depth also decreased from 15.58 μm to 11.74 μm due to the same phenomena. The as-cast and 2.5 wt.% $ZrTiO_4$ hardness values are fairly similar. It is due to the minimal interaction between Zr & Ti atoms when combined and finally does not alter the microstructure of the $ZrTiO_4$ added sample (He et al., 2010). Numbers of researchers are working on oxide-added aluminum alloys. They found that in the case of 2.5 wt.% ZrO_2 added sample shows better mechanical properties at cost of ductility.

Table 5 Mechanical properties of Al 7075; a) as-cast, b) 2.5 wt.% added ZrO_2, c) 2.5 wt.% added TiO_2, d) 2.5 wt.% added $ZrTiO_4$.

Mech. Properties	a	B	c	D
Hardness (BHN)	59	112	103	60
Micro-hardness (HV)	78	137	133	86
Micro-hardness indentation depth (μm)	15.58	11.74	11.91	14.82
Tensile Strength (MPa)	183	196	170	168
Elongation (%)	10%	3%	3%	8%

Compare to hardness values, the tensile strength trend is different. The tensile strength of the 2.5 wt.% ZrO_2 added Al7075 is 196 MPa, which is not significantly higher than 183MPa of the as-cast

sample. Furthermore, as-cast Al 7075 produced significant deformation, which was lost after the addition of oxides like ZrO_2, and TiO_2 in both cases. Due to the non-reactive nature of $ZrTiO_4$, the grain size distribution pattern becomes almost similar to the as-cast structure and offers better % elongation.

Conclusion

1. Oxide-added samples modified the microstructure by changing the distribution pattern of non-equilibrium eutectic solid solution and finer the α(Al) grains.
2. The presence of α(Al) matrix coupled with dense and discontinuous eutectic with a cluster of micro-porosities at discrete location results in loss of mechanical properties in the case of 2.5 wt.% TiO_2 added Al 7075.
3. SEM-EDS examination of ZrO_2 added Al 7075 revealed the presence of 0.22 wt.% Zr, which hinders the recrystallization of the α(Al) grains; additionally, dark spots confirm the presence of non-equilibrium eutectic phases, η($MgZn_2$), T($Al_2Mg_3Zn_3$), S(Al_2CuMg), and θ(Al_2Cu).
4. The mechanical properties are influenced by the distribution of the intermetallic phase. ZrO_2 addition offers a 52% higher hardness value compared to as-cast 7075 Al alloy. Tensile strength values remain all most same in all cases.

References

Alagarsamy, S. V., & Ravichandran, M. (2019). Synthesis, microstructure and properties of TiO2 reinforced AA7075 matrix composites via stir casting route. *Materials Research Express*, *6*(8). https://doi.org/10.1088/2053-1591/ab1d3b

ALTUNTAŞ, O. (2022). Enhancement of impact toughness properties of Al 7075 alloy via double aging heat treatment. *Gazi Üniversitesi Fen Bilimleri Dergisi Part C: Tasarım ve Teknoloji*, *10*(2). https://doi.org/10.29109/gujsc.1108116

Anyalebechi, P. N. (2004). Effects of alloying elements and solidification conditions on secondary dendrite arm spacing in aluminum alloys. *Proceedings of the TMS Fall Extraction and Processing Conference*, *2004*(January 2004), 217–233.

Chen, X. H., Yan, H., & Jie, X. P. (2015). Effects of ti addition on microstructure and mechanical properties of 7075 alloy. *International Journal of Cast Metals Research*, *28*(3), 151–157. https://doi.org/10.1179/1743133614Y.0000000137

Fan, X. G., Jiang, D. M., Meng, Q. C., Zhang, B. Y., & Wang, T. (2006). Evolution of eutectic structures in Al-Zn-Mg-Cu alloys during heat treatment. *Transactions of Nonferrous Metals Society of China (English Edition)*, *16*(3), 577–581. https://doi.org/10.1016/S1003-6326(06)60101-5

Fan, X., Jiang, D., Meng, Q., & Zhong, L. (2006). The microstructural evolution of an Al-Zn-Mg-Cu alloy during homogenization. *Materials Letters*, *60*(12), 1475–1479. https://doi.org/10.1016/j.matlet.2005.11.049

Gan, G. S., Gao, Q., Yang, B., & Gan, S. De. (2014). Effect sedimentation of TiB2 particles on the microstructure of 7075 Al alloy. *Advanced Materials Research*, *904*, 50–53. https://doi.org/10.4028/www.scientific.net/AMR.904.50

Ghosh, A., Ghosh, M., Seikh, A. H., & Alharthi, N. H. (2020). Phase transformation and dispersoid evolution for Al-Zn-Mg-Cu alloy containing Sn during homogenisation. *Journal of Materials Research and Technology*, *9*(1), 1–12. https://doi.org/10.1016/j.jmrt.2019.08.055

Ghosh, G., & Asta, M. (2005). First-principles calculation of structural energetics of Al-TM (TM = Ti, Zr, Hf) intermetallics. In *Acta Materialia* (Vol. 53, Issue 11, pp. 3225–3252). https://doi.org/10.1016/j.actamat.2005.03.028

He, Y., Zhang, X., & Cao, Z. (2010). Effect of minor Cr, Mn, Zr, Ti and B on grain refinement of as-cast Al-Zn-Mg-Cu alloys. *Xiyou Jinshu Cailiao Yu Gongcheng/Rare Metal Materials and Engineering*, *39*(7), 1135–1140. https://doi.org/10.1016/s1875-5372(10)60108-7

Ii, Y., Li, P., Zhao, G., Liu, X., & Cui, J. (2005). The constituents in Al-10Zn-2.5Mg-2.5Cu aluminum alloy. *Materials Science and Engineering A*, *397*(1–2), 204–208. https://doi.org/10.1016/j.msea.2005.02.013

Imran, M., & Khan, A. R. A. (2019). Characterization of Al-7075 metal matrix composites: A

review. *Journal of Materials Research and Technology*, *8*(3), 3347–3356. https://doi.org/10.1016/j.jmrt.2017.10.012

Kamali, H., Kamali, E., & Emamy, M. (2022). Effects of Zr additions on structure and tensile properties of an Al-4.5Cu-0.3Mg-0.05Ti (wt.%) alloy. *China Foundry*, *19*(1), 9–16. https://doi.org/10.1007/s41230-022-1094-2

Karunanithi, R., Ghosh, K. S., & Bera, S. (2014). Synthesis and characterization of TiO2 dispersed Al 7075 micro- and nanocomposite. *Advanced Materials Research*, *984–985*, 313–318. https://doi.org/10.4028/www.scientific.net/AMR.984-985.313

Li, T., Wang, S. C., & Zheng, K. H. (2015). Effect of Al-5Ti-1B grain refiner on microstructure and mechanical properties of 7075 aluminum alloy. *Materials Science Forum*, *817*, 331–336. https://doi.org/10.4028/www.scientific.net/MSF.817.331

Li, X. M., & Starink, M. J. (2001). Effect of compositional variations on characteristics of coarse intermetallic particles in overaged 7000 aluminium alloys. *Materials Science and Technology*, *17*(11), 1324–1328. https://doi.org/10.1179/026708301101509449

Mondal, C., & Mukhopadhyay, A. K. (2005). On the nature of T(Al2Mg3Zn3) and S(Al2CuMg) phases present in as-cast and annealed 7055 aluminum alloy. *Materials Science and Engineering A*, *391*(1–2), 367–376. https://doi.org/10.1016/j.msea.2004.09.013

Mondal, C., Mukhopadhyay, A. K., Raghu, T., & Varma, V. K. (2007). Tensile properties of peak aged 7055 aluminum alloy extrusions. *Materials Science and Engineering A*, *454–455*, 673–678. https://doi.org/10.1016/j.msea.2006.10.138

Morere, B., Shahani, R., Maurice, C., & Driver, J. (2001). The influence of Al3Zr dispersoids on the recrystallization of hot-deformed AA 7010 alloys. *Metallurgical and Materials Transactions A: Physical Metallurgy and Materials Science*, *32*(3), 625–632. https://doi.org/10.1007/s11661-001-0079-9

Osamura, K., Kohno, K., Okuda, H., Ochiai, S., Kusui, J., Fujii, K., Yokoe, K., Yokote, T., & Hono, K. (1996). Mesoscopic structure of super-high strength P/M Al-Zn-Mg-Cu alloys. *Materials Science Forum*, *217–222*(PART 3), 1829–1834. https://doi.org/10.4028/www.scientific.net/msf.217-222.1829

Park, J. K., & Ardell, A. J. (1988). Precipitate microstructure of peak-aged 7075 Al. *Scripta Metallurgica*, *22*(7), 1115–1119. https://doi.org/10.1016/S0036-9748(88)80114-5

Parsania, T., Thakkar, M., More, A., Mahant, D., & Rao, V. (2015). Study on Modified heat treatment of Direct Chill Cast 7075. *International Journal of Emerging Technology and Advanced Engineering*, *5*(11), 246–250. https://ijetae.com/files/Volume5Issue11/IJETAE_1115_43.pdf

Pourkia, N., Emamy, M., Farhangi, H., & Ebrahimi, S. H. S. (2010). The effect of Ti and Zr elements and cooling rate on the microstructure and tensile properties of a new developed super high-strength aluminum alloy. *Materials Science and Engineering A*, *527*(20), 5318–5325. https://doi.org/10.1016/j.msea.2010.05.009

Rao, V. J., Das, Y., & Sehgal, M. (2012). Effect of Addition of MnO 2 and Mg in LM25 Alloy. *Indian Foundry Journal*, *58*(10), 3–6.

Reza, A., Zhou, J., & Duszczyk, J. (2011). Microstructural Evolution During the Homogenization of Al-Zn-Mg Aluminum Alloys. *Recent Trends in Processing and Degradation of Aluminium Alloys*. https://doi.org/10.5772/34695

Sabbar, H. M., Leman, Z., Shamsudin, S. B., Tahir, S. M., Aiza Jaafar, C. N., Azmah Hanim, M. A., Ismsrrubie, Z. N., & Al-Alimi, S. (2021). Aa7075-zro2 nanocomposites produced by the consecutive solid-state process: A review of characterisation and potential applications. *Metals*, *11*(5). https://doi.org/10.3390/met11050805

Senkov, O. N., Bhat, R. B., Senkova, S. V., & Schloz, J. D. (2005). Microstructure and properties of cast ingots of Al-Zn-Mg-Cu alloys modified with Sc and Zr. *Metallurgical and Materials Transactions A: Physical Metallurgy and Materials Science*, *36*(8), 2115–2126. https://doi.org/10.1007/s11661-005-0332-8

Seyed Ebrahimi, S. H., Emamy, M., Pourkia, N., & Lashgari, H. R. (2010). The microstructure, hardness and tensile properties of a new super high strength aluminum alloy with Zr addition. *Materials and Design*, *31*(9), 4450–4456. https://doi.org/10.1016/j.matdes.2010.04.006

Sha, G., & Cerezo, A. (2005). Field ion microscopy and 3-D atom probe analysis of Al 3Zr particles in 7050 Al alloy. *Ultramicroscopy*, *102*(2), 151–159. https://doi.org/10.1016/j.ultramic.2004.09.006

Starink, M. J., & Li, X. M. (2003). A model for the electrical conductivity of peak-aged and overaged Al-Zn-Mg-Cu alloys. *Metallurgical and Materials Transactions A: Physical Metallurgy and Materials Science*, *34 A*(4), 899–911. https://doi.org/10.1007/s11661-003-0221-y

Tan, Q., Fan, Z., Tang, X., Yin, Y., Li, G., Huang, D., Zhang, J., Liu, Y., Wang, F., Wu, T., Yang, X., Huang, H., Zhu, Q., & Zhang, M. X. (2021). A novel strategy to additively manufacture 7075 aluminium alloy with selective laser melting. *Materials Science and Engineering A*, *821*(June). https://doi.org/10.1016/j.msea.2021.141638

Vlach, M., Kodetová, V., Kudrnová, H., Leibner, M., Cieslar, M., Šíma, V., Bajtošová, L., Kekule, T., Očenášek, V., & Čížek, J. (2020). Influence of Heat Treatment on Microhardness and Phase Transformations in Cast and Homogenized 7075(-Sc-Zr) Aluminium Alloys. *Diffusion Foundations*, *27*, 25–34. https://doi.org/10.4028/www.scientific.net/df.27.25

Wang, S. H., Meng, L. G., Yang, S. J., Fang, C. F., Hao, H., Dai, S. L., & Zhang, X. G. (2011). Microstructure of Al-Zn-Mg-Cu-Zr-0.5Er alloy under as-cast and homogenization conditions. *Transactions of Nonferrous Metals Society of China (English Edition)*, *21*(7), 1449–1454. https://doi.org/10.1016/S1003-6326(11)60880-7

Xie, F., Yan, X., Ding, L., Zhang, F., Chen, S., Chu, M. G., & Chang, Y. A. (2003). A study of microstructure and microsegregation of aluminum 7050 alloy. *Materials Science and Engineering A*, *355*(1–2), 144–153. https://doi.org/10.1016/S0921-5093(03)00056-X

Yang, X., Li, Y. dong, Luo, X. mei, Zhou, H. wei, Cai, Q. yong, Li, M., & Ma, Y. (2019). Microstructural evaluation and mechanical properties of 7075 aluminum alloy prepared by controlled diffusion solidification. *China Foundry*, *16*(4), 238–247. https://doi.org/10.1007/s41230-019-9059-9

Yazdian, N., Karimzadeh, F., & Tavoosi, M. (2010). Microstructural evolution of nanostructure 7075 aluminum alloy during isothermal annealing. *Journal of Alloys and Compounds*, *493*(1–2), 137–141. https://doi.org/10.1016/j.jallcom.2009.12.144

Zhai, F., Wang, L., Gao, X., Feng, Y., Zhao, S., & Wang, L. (2020). Phase evolution of a novel Al-Zn-Mg-Cu-Zr-Sm alloy during homogenization annealing treatment. *Materials Research Express*, *7*(7). https://doi.org/10.1088/2053-1591/aba6bf

Zhang, P. X., Yan, H., Liu, W., Zou, X. L., & Tang, B. B. (2019). Effect of T6 heat treatment on microstructure and hardness of nanosized Al2O3 reinforced 7075 aluminum matrix composites. *Metals*, *9*(1). https://doi.org/10.3390/met9010044

Zhang, W. L., Xiao, D. H., Li, T., Du, J. Di, & Ding, D. Y. (2019). Microstructure and mechanical properties of two-stage aged Al–Cu–Mg–Ag–Sm alloy. *Rare Metals*, *38*(1), 42–51. https://doi.org/10.1007/s12598-018-1137-4

Zhang, X., Xiao, Z., Yu, W., Chua, C. K., Zhu, L., Wang, Z., Xue, P., Tan, S., Wu, Y., & Zheng, H. (2022). Influence of erbium addition on the defects of selective laser-melted 7075 aluminium alloy. *Virtual and Physical Prototyping*, *17*(2), 406–418. https://doi.org/10.1080/17452759.2021.1990358

Zuo, M., Sokoluk, M., Cao, C., Yuan, J., Zheng, S., & Li, X. (2019). Microstructure Control and Performance Evolution of Aluminum Alloy 7075 by Nano-Treating. *Scientific Reports*, *9*(1), 1–11. https://doi.org/10.1038/s41598-019-47182-9